Jet Correlations in Fox-Wolfram Moments

Bachelor Thesis in Physics
submitted by Malte Seán Andreas Buschmann
born in Hamburg
SS 2012

This Bachelor Thesis has been carried out by Malte Seán Andreas Buschmann
at the Institute for Theoretical Physics in Heidelberg
under the supervision of
Prof. Dr. Tilman Plehn

Abstract

The task of this bachelor thesis is to work out and to understand the most important properties of the event shape observables Fox-Wolfram moments (FWM) and to apply them to the weak boson fusion (WBF) production channel of a Standard Model Higgs as well as corresponding background processes Z+jets and $t\bar{t}$ production. It is possible to show with the FWM that an extra QCD jet in the WBF process is radiated only under a small angle while an extra jet is more randomly distributed in case of the background processes.

Zusammenfassung

Das Ziel dieser Bachelorarbeit ist es die grundlegenden Eigenschaften der Observablen "Fox-Wolfram Momente"(FWM) zu erarbeiten und zu verstehen, sowie sie auf den schwachen bosonischen Fusionskanal eines Higgs-Teilchens im Standardmodell und zugehörige Hintergrundprozesse wie Z+Jets und $t\bar{t}$ Produktion anzuwenden. Mit Hilfe der FWM ist es möglich zu zeigen, dass ein zum Fusionsprozess hinzugefügter QCD Jet nur unter kleinen Winkeln abgestrahlt wird, während ein extra Jet im Falle der Hintergrundprozesse eher zufällig im Raum verteilt ist.

Contents

1 Introduction and Motivation

In 2009 the CERN Large Hadron Collider (LHC) started its work and since then the four main detector experiments ATLAS, CMS, ALICE and LHCb have been performing measurements of proton-proton collisions. In order to gain information about the elementary particles and their interactions in the Standard Model (and theories beyond the Standard Model) it is necessary to understand the final states (FS) of these collisions and their behaviour.

The LHC detectors can measure the four-momentum of particles created in such a collision. Hence, one can observe that groups of these particles having nearly the same momentum direction tend to be clustered into so-called jets. We are interested in how these jets can provide information about the hard process that took place.

One issue is that some of the most interesting processes have only a small cross section in comparison to other hard processes meaning that their probability to appear is low. In this thesis we want to focus on the weak boson fusion (WBF) production process of the Higgs. This is described in detail in Section 3. The advantage of investigating this process in order to measure properties of the Higgs are the FS particles. This is exploited to suppress the much more likely background processes. This suppression via so-called WBF kinematic cuts is described in Section 5.

In our analysis, we use the Fox-Wolfram moments (FWM) event shape observables [14] to gather information about the hard processes of the signal and background from the kinematics and correlations of the FS jets. In Section 6 we will see the definition and some of the important properties of this event shape observable.

In Section 7 we apply the FWM to Monte Carlo created events of the WBF process as well as to the associated background processes. Technical details about the generation of the events is described in Section 4. We study the final shape of the distributions and draw some conclusions about jet correlations. Especially correlations concerning QCD jets, which arise from parton radiation and subsequent shower, are of interest.

2 Theoretical Background - the Standard Model

The Standard Model is a quantum field theory which describes all known particles and their interactions. The Standard Model is well accepted because it is verified by experiment. However, it is not a complete theory. The Standard Model does not include any gravitational effects or dark matter but nevertheless reliable predictions can be made about particle interactions.

The Standard Model includes numerous elementary particles which can be divided into the two groups fermions and gauge bosons. All spin 1/2 particles are fermions and we can differentiate between fermions which carries a color charge and those which do not. Fermions with color charge are called quarks (q) and there exist six different quarks together with their anti-particle, namely the up, down, strange, charm, bottom and top quark, or in short notation u, d, s, c, b, and t quark. All quarks additionally carry an electric charge.

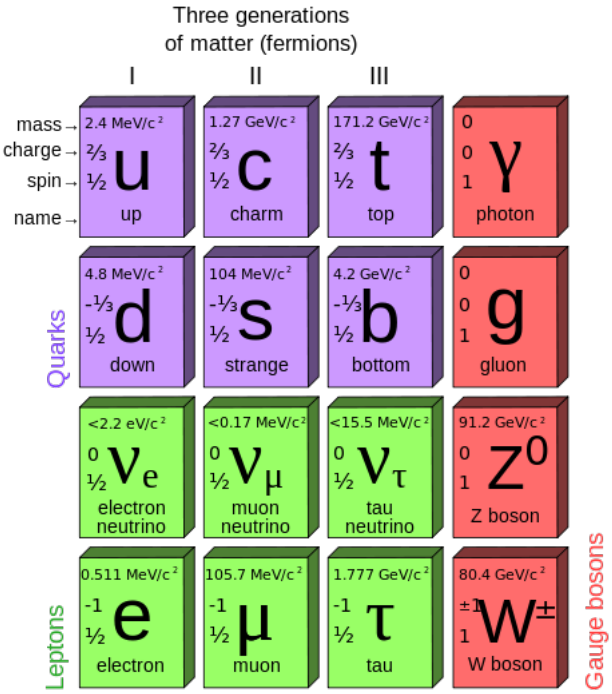

Figure 1: Overview over elementary particles . This figure is taken from [1]

Fermions without color charge are the well known leptons (l): electrons (e), muons (μ) and taus (τ) with their corresponding neutrinos (ν_l). Except neutrinos, leptons are also carrying a electric charge.

While all fermions are spin 1/2 particles gauge bosons have spin one. They are the photon (γ), the gluon (g) and the $W^{\pm}$ and Z^0 bosons. Like all gauge bosons they are known as force carriers. Recently, a new Higgs-like boson with as yet undetermined spin has recently been detected at the LHC [9][10]. The Higgs (H) is one of the

key building blocks in the Standard Model and is the only boson which not directly follows from gauge symmetry. The Higgs field was added to the Standard Model in order to maintain a proper mass term for fermions and gauge bosons otherwise they would be massless. Such a Higgs field creates masses by interacting with these particles. A summary about the existing elementary particles with the exception of the Higgs boson can be found in Figure 1.

The Standard Model describes the electromagnetic, weak and strong force, i.e. the interactions between the different group of particles. The electromagnetic force describes the interaction between charged fermions and photons while the weak force is based on the interaction with the $W^{\pm}$ and Z^0 bosons. Both forces can be described in the Standard Model by the electroweak force. The strong force is described by quantum chromodynamics (QCD) and includes all interactions between quarks and gluons thus describing color exchanges between particles. An overview between the possible interactions can be found in Table 1 below.

	l	q	g	$W^{\pm}$	Z^0	γ	H
l	×	×	×	✓	✓	✓	✓
q	×	×	✓	✓	✓	✓	✓
g	×	✓	✓	×	×	×	×
$W^{\pm}$	✓	✓	×	✓	✓	✓	✓
Z^0	✓	✓	×	✓	×	×	✓
γ	✓	✓	×	✓	×	×	×
H	✓	✓	×	✓	✓	×	✓

Table 1: Interactions between different particles of the Standard Model. See Figure 1 for the particle properties.

Color confinement states that particles with color cannot be isolated, i.e. only color neutral hadrons can exists. If e.g. two quark are separated they will decay immediately into color neutral hadrons in a process known as hadronisation. This is a common effect of hadronic collisions like those of the LHC and can be observed as a jet in the form of a spray of hadrons created by the colored particles of the hard process.

3 Particle Processes

3.1 Weak Boson Fusion Higgs Production

3.1.1 Tree Level

The signal process is that of WBF Higgs production. In this process a Standard Model Higgs boson is created via a weak interaction as it can be seen in Figure 2. The carrier of the weak force is in our case a $W^{\pm}$ boson pair which are created through weak boson bremsstrahlung from the incoming partons.

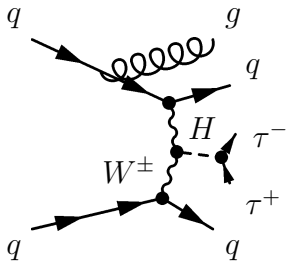

Figure 2: WBF and decay to $\tau\bar{\tau}$

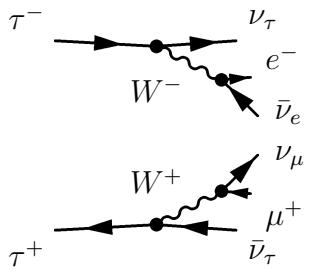

Figure 3: Leptonic $\tau^{\pm}$ decay

The Higgs boson will decay afterwards before reaching the detector. There are different decay channels possible like $H \to \gamma\gamma$ or $H \to ZZ$, but here we consider the Higgs boson to decay leptonically into a $\tau^{\pm}$ pair:

$$H \to \tau^{+}\tau^{-}. \tag{3.1}$$

Due to their short lifetimes, the created $\tau^{\pm}$ pair is not stable and the τ's will normally decay into quarks which hadronise or leptonically. Here we focus on the leptonic decay as this will give rise to a clean characteristic signal in the detector:

$$\tau^{+}\tau^{-} \to e^{\pm}\mu^{\mp}\not{p}_{T}. \tag{3.2}$$

$\not{p}_{T}$ denotes in this case missing energy in the form of the corresponding neutrinos created in this decay, which are invisible in the detector because of their weak interaction with matter.

Due to their stability, the muons and electrons they can be detected in the detector directly. However the outgoing partons which have radiated the $W^{\pm}$ bosons will hadronise to jets and therefore can not be detected directly.

As mentioned in the Introduction, we are only interested in the jet kinematics and therefore we can ignore the $\tau^{\pm}$ decay because it will have no influence on the jets. In the following analysis then, we will regard the τ's as stable. The cross section

of the overall process is reproduced by multiplying the cross section of the process without decaying τ's with the branching ratio of $\tau \to l\bar{\nu}_l$ where $l = e, \mu$.

$$\sigma_{e^\pm\mu^\mp} = \frac{B(\tau^- \to l^-\bar{\nu}_l\nu_\tau)B(\tau^+ \to l^+\nu_l\bar{\nu}_\tau)}{2}\sigma_{\tau^\pm} \tag{3.3}$$

The numerical value of the branching ratios are 0.3524 [12] and so the conversion factor is $\frac{0.3524^2}{2}$.

3.1.2 Considering an Additional QCD Jet

In addition to the process above, we also consider the possibility of one extra parton radiated at any stage of this process via the strong interaction. This extra parton will hadronise and, depending on how we characterise the jet, an additional jet may be formed. A jet produced via this QCD radiation is referred to as a QCD jet. Just how often a new jet is produced (given our jet definition) will be shown in Section 5.3. In case of such an extra jet, the WBF process could also have been gluon initiated. This can be illustrated by Figure 2 by switching the upper incoming quark with a gluon which splits to a $q\bar{q}$ pair with the (anti)quark participating in the hard process and the other parton of the pair acting as the so-called QCD radiation.

How the topological structure of this process looks like is now the important question. There are two leading jets created by the two outgoing quarks which should be still boosted along the z-direction. We expect them to be close to the beam axis. The Higgs boson instead will decay into two τ's which are more likely perpendicular to the beam axis. In case of a QCD jet the extra parton will be more likely radiated under a small angle close to the outgoing quarks and so will be the jet. So we expect between two and three jets close to the beam axis.

3.2 Backgrounds

The WBF of the Higgs can be identified in the detector by the clean central $e^\pm\mu^\mp$ pair. Further, we do not expect any hadronic activity in this region. However, there exist some other processes which will have the same characteristic signal in the form of a central $e^\pm\mu^\mp$ pair. We wish to avoid misidentifying this with a WBF process. In the following we will focus on two so called background processes, namely Z+jets and $t\bar{t}$ production.

3.2.1 Z+jets

In this background process the $e^\pm\mu^\mp$ pair is created via a decay of a Z boson into a $\tau^\pm$ pair where the τ's decay identically as in WBF:

$$qq \to Z \to \tau^+\tau^- \tag{3.4}$$

As the two extra jets of Z+jets are produced by QCD radiation, we wish to investigate how the jets of this process can mimic those of the WBF signal. These

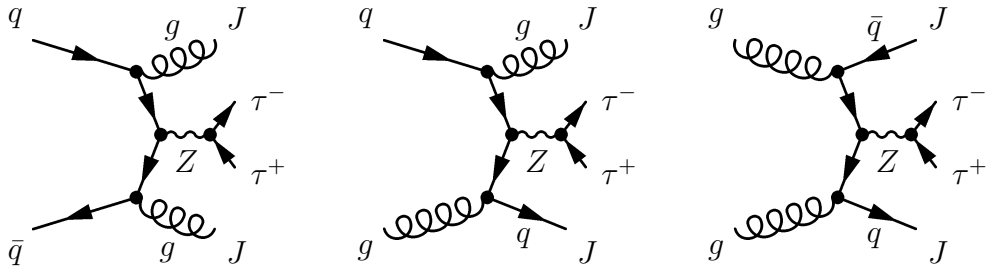

Figure 4: Example $q\bar{q}$-, gq-, and gg-initiated process with the decay to a $\tau^{\pm}$ pair

QCD jets will tend to be distributed more randomly (as will be shown) than those of WBF, giving us a handle on how to suppress this background. If we have at least one extra jet this process can also be gluon initiated as it can be seen in Figure 4.

3.2.2 $t\bar{t}$ production

Another background is known as $t\bar{t}$ production where the $e^{\pm}\mu^{\mp}$ pair is not created with a τ decay but through multiple decays initiated by the hard process $t\bar{t}$ pair. The process for the production of the $t\bar{t}$ is in general

$$pp \to t\bar{t} \tag{3.5}$$

so it can be either gluon or quark initiated.

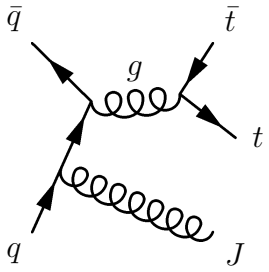

Figure 5: One of the possible $t\bar{t}$ productions

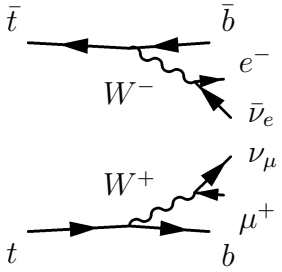

Figure 6: One possible decay of the $t\bar{t}$ pair

The decay channel for the $t\bar{t}$ pair is a decay into b quarks and a $W^{\pm}$ pair

$$pp \to t\bar{t} \to b\bar{b}W^+W^- \tag{3.6}$$

where the b quarks will hadronise and form a jet.

The $W^{\pm}$ bosons will decay leptonically into the $e^{\pm}\mu^{\mp}$ pair so finally:

$$pp \to t\bar{t} \to b\bar{b}W^+W^- \to e^{\pm}\mu^{\mp}\not{p}_T + jj \tag{3.7}$$

We will have then - like in the WBF process - two leading jets from the b quarks, but the main difference is, that this two jets are expected to be more likely central. As we have QCD radiation possibly giving rise to an extra (non-b) jet we will expect also a randomly distributed jet. Again, we use this as a way to suppress this background.

4 Technical Details

4.1 Event Generation with SHERPA

In order to theoretically study event shape observables, we use a Monte-Carlo event generator to generate events for the signal and background processes. We have used the generator SHERPA [16].

SHERPA requires a control file which takes in different options for the hard process. An example of the important parts of such a control file can be found in the following. This code snippet contains the settings of the WBF process described in the section above, including descriptive comments.

All particles are labeled following the Monte Carlo particle numbering scheme [15]. The most important numbers are ± 15 for $\tau^{\mp}$, 25 for the Standard Model Higgs and 23,± 24 for Z,$W^{\pm}$. 93 is an internal placeholder for partons.

```
// general information for SHERPA
(run){
  EVENTS 50000;      // number of events to be generated
  MASS[25]=125. // set the mass of the Higgs boson to 125 GeV
  MASSIVE[15]=1 // define the tau's to be massive
  ACTIVE[23]=0 // disable a WBF via a Z boson
  STABLE[15]=1; // set the tau's to stable
  RANDOM_SEED1=10100;     // some random seeds for ...
  RANDOM_SEED2=10001;     // ... the random number generator
  HEPMC2_SHORT_OUTPUT=event_record ;  // define the ...
  EVENT_MODE=HepMC_Short; // ... event record output mode
  EVT_FILE_PATH=/$path/
}(run);

// define the underlaying theory
(model){
  MODEL=SM;   // Standard Model is the theory ...
   // ... we want to use for our analysis
  CKMORDER=3; // we want to use the highest known order ...
   // ...in the CKM matrix elements
}(model);

// definition of the hard process
(processes){
  Process 93 93 -> 25[a] 93 93 93{1} // two incoming partons
   // -> H + two partons + one extra QCD parton
    Decay   25[a] -> -15 15       // define the Higgs to decay ...
     // ... into a tau pair
  CKKW sqrt(30/E_CMS) // set some accuracies
  Integration_Error 0.02 {4,5};
  ME_QED=Off; // avoid additional radiation of the tau's
```

```
  YFS_MODE=0;
  Order_EW 4; // number of weak interactions
  End process;
}(processes);

(beam){
  BEAM_1  2212; BEAM_ENERGY_1 7000;  //input parameters for ...
        // ... the collision:
  BEAM_2  2212; BEAM_ENERGY_2 7000;  // two protons with 7 TeV
}(beam);
```

The assumed mass for the Higgs boson is 125 GeV which is comparative close to the latest results at the LHC detectors ATLAS [9] and CMS [10].

SHERPA will calculate the cross section of the given process and afterwards events will be generated. These events will be stored in a file using HepMC2 [11]. The HepMC2 output consists of a record of all particles produced during the event - the so-called "event record".

Especially for the background processes we have to generate a very large number of events and in order to do so in appropriate amount of time we have used the bwGRiD [2]. In this way, it was possible run over 160 instances of SHERPA at the same time. The high number of events also led to a huge amount of data and we had to convert the HepMC2 format into smaller files containing only the FS particles produced in the event.

Approximately 1.3 million event of the WBF process, 110 million of Z+jets and 30 million of $t\bar{t}$ production events were generated corresponding to a total of 488 GB of data.

4.2 Event Analysis - Technical Details

The analysis is written in C++ and because of the huge amount of data it was useful to parallelize our written source code with OpenMP [4] so that multiple CPUs are used.

The event records from HepMC2 consists of hundreds of individual FS particles. For clustering the particles of an event into jets we have used FastJet [7] with the anti-k_T algorithm [6]. The anti-k_T algorithm is a commonly used jet clustering algorithm consisting of the following steps:

1. Define a list of so called preclusters which is a list of 4-momentum-vectors ordered by their absolute value. At the beginning every particle of an event is one precluster.

2. Calculate for each precluster

$$d^i = (p_T^i)^{-2} \tag{4.1}$$

   and for each pair of preclusters

$$d^{ij} = \min(d^i, d^j)\frac{(R^{ij})^2}{R} \tag{4.2}$$

with

- the transverse momentum $p_T = \sqrt{p_x^2 + p_y^2}$,
- the angular distance $R^{ij} = \sqrt{(\Delta y)^2 + (\Delta\varphi)^2}$
- where $\Delta y = y_1 - y_2$ is the difference in the rapidity $y = \frac{1}{2} \ln \frac{E+p_z}{E-p_z}$
- and $\Delta\varphi$ as the difference in azimuthal angle φ of the preclusters in spherical coordinates,
- and a free parameter R.

All of these parameters are explained in detail in the next section.

3. Determine the minimal values

$$d_{\min} = \min(d^i, d^{ij}) \tag{4.3}$$

4. If $d_{\min}$ is one of the d^{ij} than both preclusters i and j are close enough to be denoted as one single precluster. Both preclusters are merged by adding their 4-momentum and the procedure starts at point 2 again, otherwise continue with the next step.

5. $d_{\min}$ is one of the d^i which we now define as a jet. We remove this precluster from the list and continue with step 2 if preclusters are left. Otherwise all particles are already clustered to jets and we have finished.

We have used in our analysis $R = 0.4$.

The results of the calculation of important parameters are again stored in files in order to make plots afterwards. Unless otherwise noted, all plots were made with the Root package [5]. The Feynman graphs are made with the LaTeXpackage FeynMF [18].

5 Weak Boson Fusion Kinematic Cuts

The cross sections of the processes - calculated by SHERPA - are 17.2 fb for WBF, 116 pb for Z+jets and 16.9 pb for the $t\bar{t}$ production with the already applied conversion factor for the τ decay. In order to enhance the WBF signal the background is normally reduced by numerous conditions on the FS jets, i.e. events which are not fulfilling one of these conditions will not be taken into account for further analysis.

These cuts consider the kinematics of the jets and leptons and are optimized to WBF processes and the geometric characteristics of the LHC detectors. The idea is that most of the WBF events should fulfill the conditions but the background events should not. The parameters which describe the important kinematic properties of the jets are described in Section 5.1. In Section 5.2 the cuts are explained in detail.

5.1 Important Parameters

There exist two main parameters describing the kinematics of a FS object: The transverse momentum p_T and the rapidity y.

The transverse momentum p_T is simply defined as the absolute value of the momentum relative to the beam axis, z,

$$p_T = \sqrt{p_x^2 + p_y^2}, \tag{5.1}$$

if $\vec{p}_{jet} = (p_x, p_y, p_z)^T$. For low values of p_T the jet is close to the beam axis and/or it is a jet with low total momentum. If the FS object is a jet, we will refer to this as soft jet. A high p_T instead indicated a very high total momentum and/or an object nearly perpendicular to the beam axis. If a jet, it is named a hard jet.

The rapidity y describes how close a jet is to the beam axis and is defined by

$$y = \frac{1}{2} \ln \frac{E + p_z}{E - p_z}, \tag{5.2}$$

with E the energy. In the massless case, the rapidity is then called pseudorapidity and can be shown to take the form $\eta = -\ln \tan \frac{\theta}{2}$, and is now only a function of the polar angle θ. Rapidity y is zero for an object completely perpendicular to the beam axis, whereas y goes to infinity for an object parallel to the beam axis. Objects tending toward zero rapidity are called central while objects with very large positive or negative rapidity are called forward or backward, respectively.

A third important parameter is the angular distance $\Delta R_{j_1 j_2}$ between two objects,

$$\Delta R_{j_1 j_2} = \sqrt{(\Delta y)^2 + (\Delta \varphi)^2} \tag{5.3}$$

where $\Delta\varphi = \varphi_{j_1} - \varphi_{j_2}$ is the difference in azimuthal angle of the two objects j_1 and j_2, and $\Delta y = y_{j_1} - y_{j_2}$. With the definition of the invariant mass

$$M_{j_1 j_2} = \sqrt{(\Delta E)^2 - (\Delta \vec{p})^2}. \tag{5.4}$$

the set of important parameters for kinematic cuts is complete.

5.2 Description of Cuts

The specific cuts mainly follow the work of [19]. The first two cuts were applied to the leptons, so either $\tau^{\pm}$ for WBF and Z+jets or the $e^{\pm}\mu^{\mp}$ pair in case of $t\bar{t}$ production:

$$p_{T,l} \leq 10 \text{ GeV} \qquad \text{and} \tag{5.5}$$

$$|y_l| \geq 2.5 \tag{5.6}$$

The first cut claim the leptons to fulfill a quite minimal p_T requirement, whereas the second one ensures the leptons to be central. Both cuts mainly lead to a very clean signal in the detector so that these processes can be identified easily.

The third cut is applied to the jets. The condition is that there must exist at least two jets which fulfill

$$p_{T,j} \geq 20 \text{ GeV} \qquad \text{and} \tag{5.7}$$

$$|y_j| \leq 5.0. \tag{5.8}$$

This rapidity cut has to be performed because of the geometry of the detector. As long as it is not possible to build a detector in front of the beam tunnel, the jets close to beam axis can't be measured. This leads to the demand that the rapidity must be lower than a certain value, in this case 5.0. The p_T cut ensures that there are at least two detectable jets. The following cuts are only applied to the two hardest jets, j_1 and j_2, which fulfill the above condition. These are furthermore referred to as 'tagging jets'.

The next two cuts guarantee that these two jets are well separated, both from each other and from the leptons.

$$\Delta R_{j_1 j_2} \leq 0.7 \qquad \text{and} \tag{5.9}$$

$$\Delta R_{jl} \leq 0.7 \tag{5.10}$$

This is due to resolution limits of the detector and to avoid incorrect identification of the two leptons.

The up to now performed cuts are mainly done to get a clean characteristic detector signal and to minimally isolated jets from each other and the leptons. The following cuts are meant to distinguish between WBF and the background processes with the aim of suppressing the background.

This next requirement ensures that both leptons are more central than the two hardest jets and that the leptons are in between these two jets in reference to the θ plane:

$$\min(y_{j_1}, y_{j_2}) + 0.7 < y_l < \max(y_{j_1}, y_{j_2}) - 0.7 \tag{5.11}$$

This condition is generally true for WBF, because we expect the leptons to be central and the jets to be forward or backward but not necessarily for the $t\bar{t}$ production

process where the jets coming from the hadronised b-quarks tending to be more central.

It is necessary that all events contain tagging jets in opposite hemispheres:

$$y_{j_1} \cdot y_{j_2} < 0, \tag{5.12}$$

Next, we require the tagging jets to have a minimal separation in rapidity of 4.4 units.

$$|y_{j_1} - y_{j_2}| \geq 4.4. \tag{5.13}$$

For forward and backward jets in different hemispheres, as it is the case in WBF, it is easy to see that this condition is generally fulfilled. This will be shown explicitly in the next section using a cut flow analysis.

The next to last cut claims the invariant mass of the two jets be higher than a certain value:

$$M_{j_1 j_2} \geq 600 \text{ GeV} \tag{5.14}$$

Additionally there is on more cut applied known as a b-veto. At the LHC it is possible to tag jets which are coming from hadronised b quarks and therefore to exclude $t\bar{t}$ production events, see for example [8] for further information in case of the ATLAS experiment. We can simulate such a b-veto by demanding a central b quark

$$p_{T,b} \geq 20 \text{ GeV} \qquad \text{and} \tag{5.15}$$

$$y_b \leq 2.5 \tag{5.16}$$

and ignore such an event with a possibility of 60%. These 60% refers to the success rate of a b-tag.

5.3 Cut Flow Analysis

In Table 2 are the results of these cuts and we can see that the cross sections of the background processes are much lower than before. Even though the cross section of WBF is still lower than the cross sections of Z+jets and $t\bar{t}$ production they now span only two order of magnitude, rather than up to five initially. In total, 161 765 of WBF, 34 865 of Z+jets and 36 048 of $t\bar{t}$ events survive the cuts and are used for further analysis.

In Table 3 we can see how many events with a certain number of jets are existing as well as the average. WBF and Z+jets are mainly consisting of 2-jet and 3-jet events while in case of $t\bar{t}$ production higher jet multiplicities are observed.

Acceptance Criteria	Non-Survival Probability [%]			cross section [fb]		
	WBF	Z+jets	$t\bar{t}$	WBF	Z+jets	$t\bar{t}$
$p_{T,l} \geq 10$ GeV	2.9	6.1	9.4	16.7	109 000	15 400
$\lvert y_l \rvert \leq 2.5$	23.3	47.7	14.2	12.8	57 100	13 200
$p_{T,j} \geq 20$ GeV and $\lvert y_j \rvert \leq 5.0$	31.2	91.9	6.8	8.8	4 640	12 300
$\Delta R_{j_1 j_2} \geq 0.7$	3.2	4.5	2.4	8.5	4 430	12 000
$\Delta R_{jl} \geq 0.7$	8.2	15.0	20.0	7.8	3 770	9 600
$\min(y_{j_1}, y_{j_2}) + 0.7 < y_l$ and $\max(y_{j_1}, y_{j_2}) - 0.7 > y_l$	50.6	92.3	94.0	3.9	289	574
$y_{j_1} \cdot y_{j_2} < 0$	3.9	13.8	13.6	3.7	249	496
$\lvert y_{j_1} - y_{j_2} \rvert \geq 4.4$	26.9	63.9	78.7	2.7	90.0	105
$M_{j_1 j_2} \geq 600$ GeV	19.1	58.7	32.4	2.2	37.2	71.3
$p_{T,b} \geq 20$ GeV and $y_b \leq 2.5$			70.6			20.9

Table 2: Cut flow for WBF and its backgrounds with the resultant cross sections. The cross section of the processes with stable τ's have been multiplied with the conversion factor $\frac{0.3524^2}{2}$, so that they can be compared directly with the $t\bar{t}$ process.

number jets	WBF	Z+jets	$t\bar{t}$ production
2	85.0%	64.7%	25.4%
3	13.4%	24.5%	32.2%
4	1.5%	7.9%	23.2%
5	0.1%	2.2%	12.2%
>5	0.1%	0.7%	6.9%
Ø	2.2 jets	2.5 jets	3.5 jets

Table 3: Amount of jets in an event for the different processes after all acceptance criteria are met.

6 Fox-Wolfram moments

6.1 General Properties

6.1.1 Definition

The FWM are a set of event shape variables originally defined as

$$H_l = \frac{4\pi}{2l+1} \sum_{m=-l}^{l} \left| \sum_i Y_l^m(\varphi_i, \theta_i) \frac{|\vec{p}_i|}{\sqrt{s}} \right|^2 \tag{6.1}$$

and are first introduced by Geoffrey C.Fox and Stephen Wolfram for $e^{\pm}$ annihilations in 1979 [14]. Y_l^m denotes the spherical harmonics, $|\vec{p}_i|$ refers to the absolute value of the momentum of the FS jets, $\sqrt{s} = \sum_i |\vec{p}_i|$ is the total available momentum of the jets and φ_i/θ_i are the azimuthal and polar angle, respectively, of the jets in common spherical coordinates. Notice that s is in this case not the Madelstam variable which would include the total four momentum.

A more useful expression is the above formula in terms of the Legendre polynomials P_l:

$$H_l = \frac{4\pi}{(2l+1)\cdot s} \sum_{m=-l}^{l} \left| \sum_i Y_l^m(\varphi_i, \theta_i) \, |\vec{p}_i| \right|^2 \tag{6.2}$$

$$= \frac{4\pi}{(2l+1)\cdot s} \sum_{m=-l}^{l} \left(\sum_i Y_l^m(\varphi_i, \theta_i) \, |\vec{p}_i| \right) \left(\sum_j Y_l^{*m}(\varphi_j, \theta_j) \, |\vec{p}_j| \right) \tag{6.3}$$

$$= \sum_{i,j} \frac{4\pi \, |\vec{p}_i| \, |\vec{p}_j|}{(2l+1)\cdot s} \sum_{m=-l}^{l} Y_l^m(\varphi_i, \theta_i) Y_l^{*m}(\varphi_j, \theta_j) \tag{6.4}$$

$$= \sum_{i,j} \frac{|\vec{p}_i| \, |\vec{p}_j|}{s} P_l(\cos\Omega_{ij}) \tag{6.5}$$

where in the last line the addition theorem for the spherical harmonics

$$P_l(\cos\Omega_{ij}) = \frac{4\pi}{(2l+1)} \sum_{m=-l}^{l} Y_l^m(\varphi_i, \theta_i) \cdot Y_l^{*m}(\varphi_j, \theta_j) \tag{6.6}$$

is used with Ω_{ij} as the total angle between jet i and jet j.

6.1.2 Weight Factors

Deviating from the original definition it might be also interesting to define the FWM with p_T instead of $|\vec{p}|$ as a weight factor in front of the Legendre polynomials [13]. For this purpose we will write in the following W_i instead of $|\vec{p}_i|$ as a general placeholder for the different definitions:

$$H_l = \sum_{i,j} \frac{W_i W_j}{s} P_l(\cos\Omega_{ij}) \tag{6.7}$$

Notice that in this case also the normalization factor s has to be varied in order to be consistent, so $\sqrt{s} = \sum_i W_i$.

6.1.3 Legendre Polynomials

The rewritten FWM depend on the Legendre polynomials so it is important to know how they look like. In Figure 7 is a plot of the first six Legendre polynomials which are defined as

$$P_l(x) = \frac{1}{2^l l!} \frac{d^l}{dx^l} \left[\left(x^2 - 1\right)^l \right] \tag{6.8}$$

$$P_0(x) = 1 \tag{6.9}$$

$$P_1(x) = x \tag{6.10}$$

$$P_2(x) = \frac{1}{2} \left(3x^2 - 1\right) \tag{6.11}$$

$$\vdots \tag{6.12}$$

$$P_5(x) = \frac{1}{8} \left(63x^5 - 70x^3 + 15x\right) \tag{6.13}$$

In our calculations we have made use of the recursive relation, known as the Bonnet's recursive formula:

$$(l+1)P_{l+1}(x) = (2l+1)xP_l(x) - lP_{l-1}(x) \tag{6.14}$$

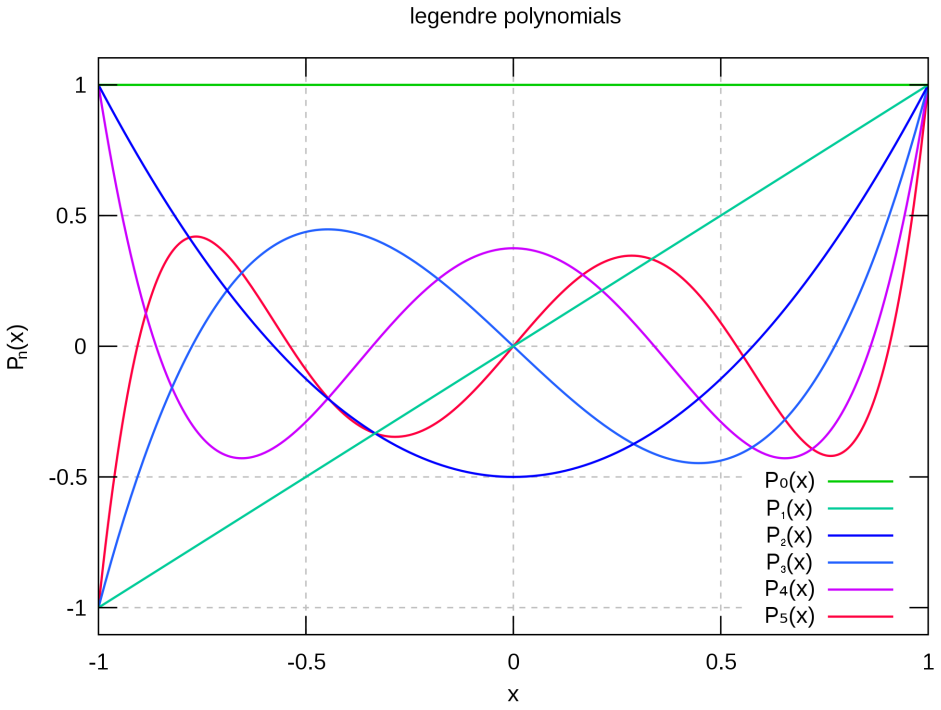

Figure 7: The first Legendre polynomials. This figure is taken from [3]

One can see that the Legendre polynomials for odd l are odd and even for even l. For an angle of $\Omega_{ij} = 180°$ between two jets, $\cos\Omega_{ij} = -1$ and hence the Legendre polynomials will take the value $(-1)^l$. In the case of WBF the two tagging jets will approach this case. As $\Omega_{ij} = \Omega_{ji}$ and $P_l(\Omega_{ii}) = 1$ will hold so we can split up the sum of the FWM:

$$H_l = \frac{1}{s}\left(\sum_i W_i^2 + 2\sum_{i<j} W_i W_j P_l(\cos\Omega_{ij})\right) \tag{6.15}$$

6.1.4 Boundaries

A important question concerning the FWM is whether they are bounded or not. To calculate the upper bound we could assume $P_l(\cos\Omega_{ij}) = 1$ because that is the highest possible value for the Legendre polynomials and all weight factors in front are positive:

$$H_{l,max} = \sum_{i,j}\frac{W_i W_j}{s} = \frac{\sum\limits_{i,j} W_i W_j}{\left(\sum\limits_k W_k\right)^2} = \frac{\sum\limits_{i,j} W_i W_j}{\sum\limits_{k,m} W_k W_m} = 1 \tag{6.16}$$

So this leads to the conclusion

$$H_l \leq 1. \tag{6.17}$$

Incidentally the above equation is also true for $l = 0$ because of $P_0(x) = 1$, so $H_0 = 1$ will hold for all events.

The lower bound is more difficult. $P_l(\cos\Omega_{ij}) = -1$ is the lowest possible value for the Legendre polynomials and Eq.(6.15) gets simplified to

$$H_{l,min} = \frac{1}{s}\left(\sum_i W_i^2 - 2\sum_{i<j} W_i W_j\right) \tag{6.18}$$

which in general could be smaller than zero. For only two jets this formula becomes $H_{l,min} = \frac{(W_1 - W_2)^2}{s}$ which is always greater than or equal to zero. But already for more than two jets the assumption $P_l(\cos\Omega_{ij}) = -1$ breaks down because it is not possible that every angle Ω_{ij} between the jets is 180°. So the $H_{l,min}$ from above will not be reached for more than two jets. We observe that also for more than two jets the condition $H_l \geq 0$ seems to hold. So finally we can state that:

$$0 \leq H_l \leq 1 \tag{6.19}$$

6.2 2-jet Events

6.2.1 Simplifications

The general definition of the FWM is quite unhandy because of its double sum over the jets. Therefore, it was useful to come up with some simplifications in order to get a better feeling for its properties.

First of all we will take only jets with $p_T \geq 20$ GeV and $|y| \geq 5.0$ into account. Due to the detector resolution and geometry this is a condition which we have to introduce as we have seen in the section before. This reduces the number of jets significantly, on average only 2.2 jets for WBF, 2.5 jets for Z+jets and 3.5 jets for $t\bar{t}$ production will go into the calculations of the FWM (see Table 3 of Section 5.3).

There are many events which consists only of the two tagged jets and hence the sum has only two terms. While this greatly simplifies the analysis even for three or more jet events this simplification can give an approximation because for every softer jet the weight factor W_i gets per construction smaller. In the case of just two tagging jets we can explicitly write out the sum:

$$H_l^{(\text{2-jets})} = \frac{W_1^2 P_l(\cos\Omega_{11}) + W_2^2 P_l(\cos\Omega_{22}) + 2W_1W_2 P_l(\cos\Omega_{12})}{s} \tag{6.20}$$

$$= \frac{W_1^2 + W_2^2 + 2W_1W_2 P_l(\cos\Omega_{12})}{(W_1+W_2)^2} \tag{6.21}$$

where we have used that $P_l(\cos\Omega_{ii}) = P_l(1) = 1$. This equation can be even more simplified by parameterize this formula using

$$W_2 = r \cdot W_1,\ \Omega_{12} \equiv \Omega \tag{6.22}$$

where without loss of generality $W_1 \geq W_2$ so that $r \in (0, 1]$:

$$H_l^{(\text{2-jets})} = \frac{1 + 2rP_l(\cos\Omega) + r^2}{(1+r)^2} \tag{6.23}$$

This equation effectively describes the dominant behaviour of the FWM for any number of tagging jets, as will be seen. The formula finally depends only on two parameters, namely the total angle Ω between the two jets and their ratio r in either p_T or $|\vec{p}|$, which makes it possible to draw an analytical 2-dimensional plot of this function. One advantage of this parameterization is the fixed range for the parameters because $r \in (0, 1]$ and $\Omega \in [0, \pi] \equiv [0°, 180°]$ will always hold so we are able to make this plot independent of the definition of the weight factor and with dimensionless parameters:

$$H_l^{(\text{2-jets})} : (0, 1] \times [0, \pi] \to [0, 1] \tag{6.24}$$

In Figure 8 we have done this 3-dimensional plot for several different ls and one can observe the influence of the symmetry properties of the Legendre polynomials. We can see that the influence of the parameter r is quite small in comparison to the total angle Ω. r is only important at small values, or in other words when one jet is comparatively hard. In the other cases we can reduce our focus to the angle Ω.

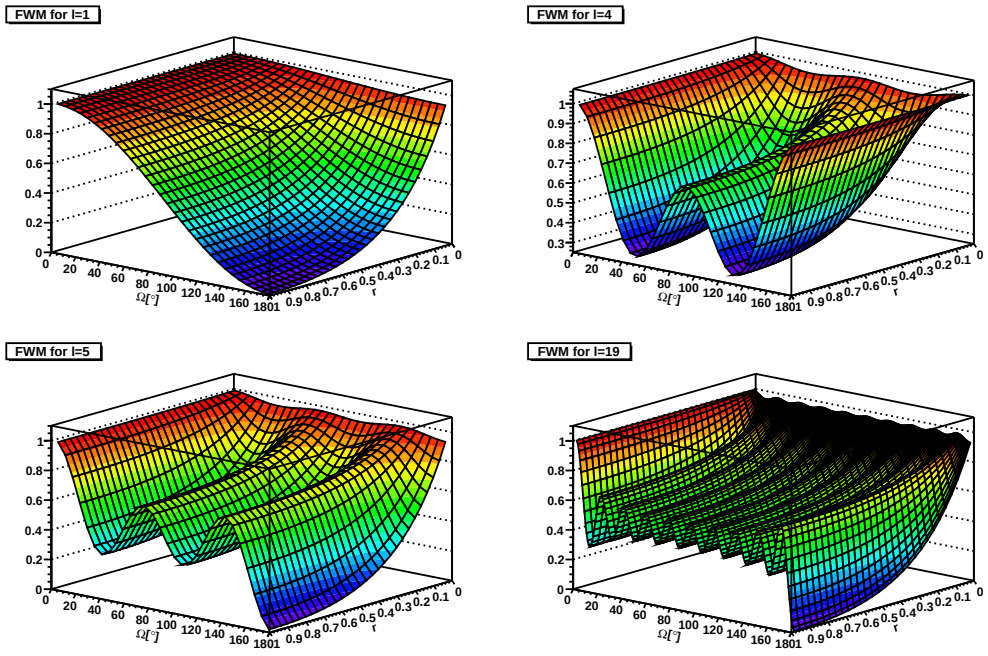

Figure 8: A plot of the analytical expression of the FWM in the 2-jet case for several values of l

6.2.2 Understanding the Shape

We now use the generated events to calculate distributions for the FWM in the limit of 2-jet events. Figure 9 shows the H_5 distribution for the signal and background after the necessary minimal cuts of eq.(5.5)-(5.8) and p_T as the weight factor. The justification of this choice of weight factor is postponed to a later section. We have applied only the minimal cuts so we expect a difference in shape between the processes because the different topological structures are still present.

Independent of the process the FWM seems to have the same characteristic shape. Each process does have two sharp cuts around 0.3 and two broad peaks around 0.7 which can be explained by looking at Figure 8:

Due to the Legendre polynomials, H_5 has two local maxima and two minima. Over a wide range of r the level of these maxima and minima are nearly the same so that we can denote them as a stationary line. The value of this stationary line can be approximated by setting $r = 1$ into eq.(6.23),

$$H_5^{(2\text{-jets})} \overset{r=1}{=} \frac{1 + 2P_5(\cos\Omega) + 1}{2^2} \tag{6.25}$$

$$= \frac{1}{2}\left(1 + P_5(\cos\Omega)\right) \tag{6.26}$$

and calculating the local extrema.

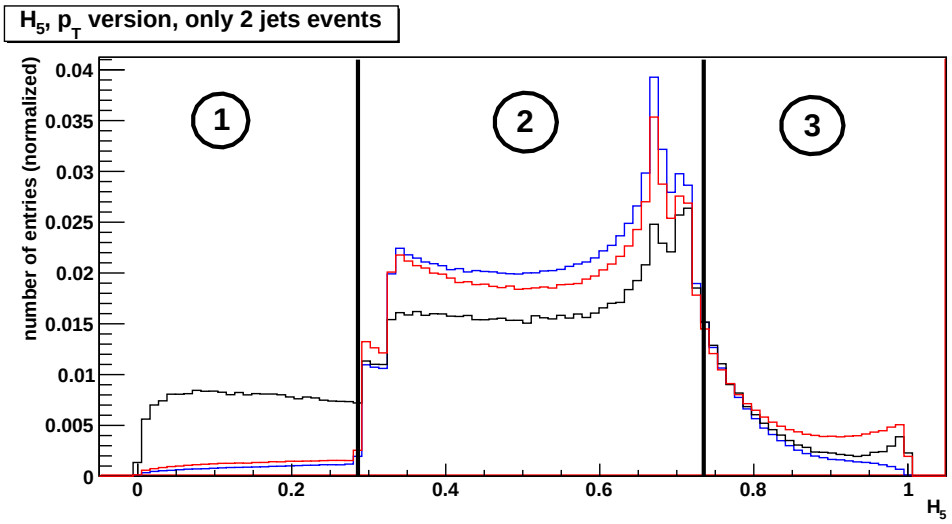

Figure 9: FWM applied to WBF (black), Z+jets (red) and $t\bar{t}$ (blue) with l=5 just after the minimal kinematic cuts. Only events with two jets are taken into account and p_T is used as the weight factor. The graph is normalized such that the sum over the bins is one.

The resultant extrema are:

$$\Omega_1 = 40^\circ \qquad \Rightarrow H_5^{(\text{2-jets})}(r=1,\Omega_1) = 0.29 \tag{6.27}$$

$$\Omega_2 = 73^\circ \qquad \Rightarrow H_5^{(\text{2-jets})}(r=1,\Omega_2) = 0.67 \tag{6.28}$$

$$\Omega_3 = 107^\circ \qquad \Rightarrow H_5^{(\text{2-jets})}(r=1,\Omega_3) = 0.33 \tag{6.29}$$

$$\Omega_4 = 140^\circ \qquad \Rightarrow H_5^{(\text{2-jets})}(r=1,\Omega_4) = 0.71 \tag{6.30}$$

We can see that these values correspond to the cuts and the peaks mentioned above and the reason is quite plausible. Around such a stationary line the dependence on the angle Ω and the ratio r is quite small in comparison to everything else where the gradient is much higher. The reason why the minima give rise to a sharp cut while the maxima have a broad peak is simply that the minima are a stable line while the maxima are unstable: When we are at a minimum and vary the angle Ω and r the value for the FWM will always grow to some approximation. Due to this behaviour values below this minima can't be reached in that local region of the r-Ω space and so a sharp border will arise. However, at a maximum we can vary the two parameters r and Ω and the FWM can get both larger and smaller depending on the direction of the variation. A smeared peak at 0.71 and 0.67 is the result.

A similar behaviour can be observed also for other odd and even l than $l = 5$ and the number and position of possible peaks and cuts depends obviously on the value for l.

The visibility of the peaks and cuts can give information on how many events are in the associated region. The higher the value for l the more minima and maxima we have in the Legendre polynomials and this leads of course to more peaks and

cuts in the FWM. Because the position of the maxima and minima changes with l it is in general possible to scan through the r-Ω space with varying l to see how many events are in a region around such a stationary line.

6.2.3 Jet Correlations

Let us first define three different regions for H_5: region 1 is the region with FWM smaller than the first sharp cut at 0.29, region 3 is the region with Fox-Wolfram a bit higher than the peak at 0.71 and region 2 is the intermediate region with FWM in between; see Figure 9.

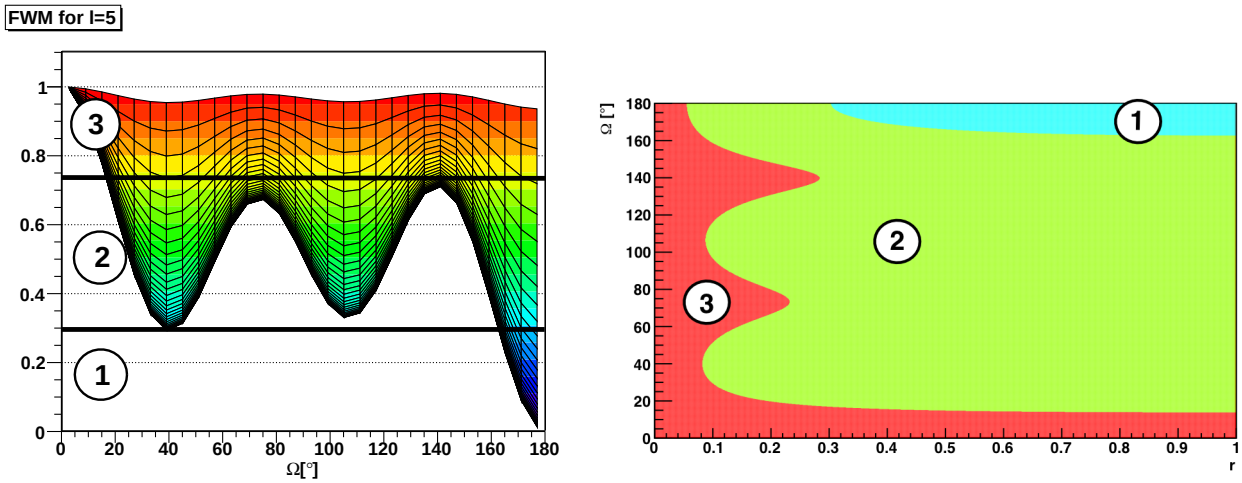

Figure 10: Visualization of the three regions for $l = 5$.
left: pure Ω dependency. The accessible region due to r is colored.
right: r-Ω plane.

The motivation of this definition is that we can deduce from the region information about the correlation between the two jets. Of course during the calculation of the FWM information is lost because H_l maps two parameters onto one (see. eq.(6.24)) but it is possible to unite the jet correlations. Note that the border between region 2 and region 3 is only roughly defined due to the broad shape of the peak. This is easily seen readily in the leftmost plot of Figure 10.

Region 1 refers to events where the two tagging jets are nearly back to back and don't have a small value for r as it can be seen in Figure 10. The WBF graph in Figure 9 is higher than e.g Z+jets which is easy to understand concerning the topological structure of the different processes: The two dominating jets of WBF should be forward-backward and thus nearly back-to-back. There does not exist a condition like this for the leading jets of Z+jets. The jets of Z+jets could be more evenly distributed and so this leads to a lower line in this region in comparison to WBF.

Events which will have a value for the FWM in region 3 have jets with nearly the opposite correlation than the jets in region 1: the jets of events in region 3 have to be nearly parallel and/or they have a small ratio r.

All other events will lay in region 2. These events will have jets which are not parallel and in addition the ratio r is not small.

We have defined these three regions for H_5 but we can define these regions in the same way also for other value of l. For odd values of l the only differences are the numerical values of the borders, because the position of the maxima and minima of the Legendre polynomials are different. In general, the sizes of region 1 and 3 will get smaller for higher odd values of l. However for even values of l there is one additional change: As the Legendre polynomials are even functions there is no difference between angles of 0° and 180°. Due to this property, events which are normally in region 1 are now overlaid with region 3. Thus, the Legendre polynomials do not allow for even l any values below region 2. A summary of the properties of this regions can be found in Table 4.

region	jet correlation odd l	jet correlation even l
1	nearly back to back, no small r	not reachable
2	not parallel, no small r	not parallel, not back to back, no small r
3	nearly parallel or small r	back to back or parallel or small r

Table 4: Three defined regions in the FWM and the associated jet correlations

We know what to expect after applying all WBF kinematic cuts: The two leading jets should be back to back to some approximation so we expect the events to be mainly in region 1 for odd l and region 3 for even l. As a result we expect a peak at zero for odd l and a peak at one for even l for the events with two jets.

Note that it is possible to gather information about the correlation between the jets but the FWM can't give any information about the position in space as long as the only parameters are r and Ω. This means that we can't differentiate between a central jet pair and a forward-backward jet pair in case of only two jets.

6.2.4 Dependence on Spherical Coordinates

With the total angle Ω the FWM depend on a parameter which is independent of the choice of a coordinate system, but many physical questions refer to the polar and azimuthal angle of the two leading jets. Thus it might be useful to express Ω in terms of spherical coordinates:

$$\cos\Omega = \frac{\vec{p}_1 \cdot \vec{p}_2}{|\vec{p}_1|\,|\vec{p}_2|} \tag{6.31}$$

with

$$\vec{p_i} = |\vec{p_i}| \begin{pmatrix} \sin\theta_i \cos\varphi_i \\ \sin\theta_i \sin\varphi_i \\ \cos\theta_i \end{pmatrix} \tag{6.32}$$

eq. (6.31) reads:

$$\cos\Omega = \sin\theta_1 \sin\theta_2 \left(\cos\varphi_1 \cos\varphi_2 + \sin\varphi_1 \sin\varphi_2\right) + \cos\theta_1 \cos\theta_2 \tag{6.33}$$

$$= \sin\theta_1 \sin\theta_2 \sin\Delta\varphi + \cos\theta_1 \cos\theta_2 \tag{6.34}$$

$$= \frac{1}{2}\left[(\cos\Delta\theta - \cos\square\theta)\sin\Delta\varphi + \cos\Delta\theta + \cos\square\theta\right] \tag{6.35}$$

where we have used the trigonometric addition theorems and $\Delta\theta := \theta_1 - \theta_2$, $\square\theta := \theta_1 + \theta_2$. So it is possible to parameterize the total angle in terms of the difference in azimuthal angle and in the sum and difference in polar angle.

However, in WBF we generally expect $\theta_1 \approx 0$ and $\theta_2 \approx \pi$ thus $\Delta\theta \approx \square\theta$ which means the pre-factor in front of $\sin\Delta\varphi$ is comparatively small with respect to the other terms. In other words, the dependence on $\Delta\varphi$ is low but still present because due to the kinematic cuts none of the jets will be completely parallel to the beam axis.

6.3 n-jet Events

After we have seen the properties of the FWM in the 2-jet case an obvious question is how much influence a larger number of jets would have. As already mentioned, the equation (6.23) for 2-jet events might give a good approximation for the FWM in the three or more jet case because per construction the p_T of the subsequent jets is smaller and also is their contribution to the FWM. The 3-jet events are of interest as this third jet most likely arises from the QCD radiation and we exactly wish to investigate correlations between QCD jets and the tagging jets.

6.3.1 Small 3rd jet

The first obvious task is to parameterize the FWM for 3-jet events as follows:

$$H_l^{(\text{3-jets})} = \frac{1 + r_2^2 + r_3^2 + 2r_2 P_l^{12} + 2r_3 P_l^{13} + 2r_2 r_3 P_l^{23}}{(1 + r_2 + r_3)^2} \tag{6.36}$$

with

$$r_2 W_1 = W_2 \qquad \text{with } r_2 \in (0, 1] \tag{6.37}$$

$$r_3 W_1 = W_3 \qquad \text{with } r_3 \in [0, r_2] \tag{6.38}$$

$$P_l^{ij} \equiv P_l(\cos\Omega_{ij}) \tag{6.39}$$

Let us now assume a vanishing third jet so that we can make a Taylor expansion around $r_3 = 0$ up to the order $\mathcal{O}(r_3)$:

$$H_l^{(\text{3-jets})} = H_l^{(\text{3-jets})}\Big|_{r_3=0} + \frac{\partial H_l^{(\text{3-jets})}}{\partial r_3}\Big|_{r_3=0} \cdot r_3 + \mathcal{O}(r_3^2) \tag{6.40}$$

$$\equiv H_l^{(\text{2-jets})} + \delta H_l^{(\text{3rd jet})} \tag{6.41}$$

where

$$\delta H_l^{(\text{3rd jet})} := \left.\frac{\partial H_l^{(\text{3-jets})}}{\partial r_3}\right|_{r_3=0} \cdot r_3 + \mathcal{O}(r_3^2) \tag{6.42}$$

$$= 2\left(\frac{P_l^{13} + r_2 P_l^{23}}{(1+r_2)^2} - \frac{1 + r_2 + 2r_2 P_l^{12}}{(1+r_2)^3}\right) \cdot r_3 + \mathcal{O}(r_3^2) \tag{6.43}$$

$$= \frac{2r_3}{(1+r_2)^2}\left(P_l^{13} + r_2 P_l^{23} - (1+r_2) H_l^{(\text{2-jets})}\right) + \mathcal{O}(r_3^2) \tag{6.44}$$

$$= \Delta + \mathcal{O}(r_3^2) \tag{6.45}$$

can denote a correction factor of $H_l^{(\text{2-jets})}$ in case of a small 3rd jet.

Due to the acceptance criteria of jets we expect no 3rd jet with $r_3 \approx 0$ thus the Taylor expansion around $r_3 = 0$ has to be justified. As long as r_3 is not zero but with an average of around 0.4 comparatively small, the only issue might be that we have to take much higher orders in r_3 into account to get sufficient results. Let us take a look at $\delta H_l^{(\text{3rd jet})}$ including $\mathcal{O}(r_3^2)$ which can be written as

$$\delta H_l^{(\text{3rd jet})} = \left(1 - \frac{2r_3}{1+r_2}\right) \cdot \Delta + 2\left(1 - P_l^{12}\right) \frac{r_2 r_3^2}{(1+r_2)^4} + \mathcal{O}(r_3^3). \tag{6.46}$$

The correction up to the third order includes two terms whereas the second one is due to the very small factor $\frac{r_2 r_3^2}{(r_2+1)^4} < 0.03$ negligible. The first term is the correction Δ of Eq. (6.45) but reduced by a factor which can not be discussed away. Even higher orders will add more smaller corrections with changing signs to Δ. Thus they are changing the scale of the correction factor $\delta H_l^{(\text{3rd jet})}$, but independent of the orientation in space of the third jet.

These corrections on Δ aren't small for the first orders in r_3 thus a quantitative analysis must include higher orders. But as long as we are not interested in the exact values of $\delta H_l^{(\text{3rd jet})}$ and the scale does not depend on orientation of the third jet in space, it is still possible to make statements about a third jet with the distribution of Eq. (6.45). However, we have to keep in mind that we overestimate the value for $\delta H_l^{(\text{3rd jet})}$.

An interesting property of this correction factor $\delta H_l^{(\text{3rd jet})}$ is that it is a function of the FWM of the two tagged jets. Thus the strength of this correction depends on the parity of l because the FWM should peak around zero for odd l and around one for even l as mentioned above.

An important remark is that in the 2-jet case there was a region for even l (region 1) which couldn't be reached due to the symmetry of the Legendre polynomials. However, in the 3-jet case it is possible that an event will be in this region.

6.3.2 Events with $n > 3$

We can make the same Taylor expansion ansatz of a small 3rd jet also for more than three jets because every additional jet is even softer. In general

$$H_l^{(\text{n-jets})} = H_l^{((\text{n-1})\text{-jets})} + \delta H_l^{(\text{n-th jet})} \tag{6.47}$$

$$= H_l^{((\text{n-2})\text{-jets})} + \delta H_l^{((\text{n-1})\text{-th jet})} + \delta H_l^{(\text{n-th jet})} \tag{6.48}$$

$$= H_l^{(\text{2-jets})} + \sum_{i=3}^{n} \delta H_l^{(\text{i-th jet})} \tag{6.49}$$

will hold with

$$\delta H_l^{(\text{i-th jet})} := \lim_{m_i \to \infty} \sum_{j=1}^{m_i} \left. \frac{\partial^j H_l^{(\text{i-jets})}}{j! \cdot \partial (r_i)^j} \right|_{r_i=0} \cdot r_i^j. \tag{6.50}$$

This formula means that we can reduce even an n-jet event to an 2-jet event which is shifted by $\delta H_l^{(\text{i-th jet})}$ with every additional jet i. An interesting observation is that the shift of the i-th jet depends only on the parameters of the harder jets even if there are softer jets existing. These shifts can be approximated by choosing an appropriate value for the order m_i but we have to keep in mind not to screw up with the order $\mathcal{O}(r_i^{m_i})$ because eq. (6.49) is not a proper Taylor expansion in multiple variables.

Due to the shrinking influence of an additional jet we expect that in most cases

$$\delta H_l^{(\text{i-th jet})} > \delta H_l^{((\text{i+1})\text{-th jet})} \tag{6.51}$$

but note that this might not be generally true. Thus we have to choose the order m_i carefully.

7 Distributions

7.1 Observations

In the last section we have discussed the most important properties of the FWM construction up to n jets. With this knowledge it is easy to understand to shape of the FWM in the 2-jet case and even in the 3-jet case. In the following we will see the FWM applied to the signal and background processes after all described kinematic cuts have been performed. We will discuss the shape of the event shape observable with references to the previous sections.

7.1.1 Weak Boson Fusion and Background

In Figure 11 and Figure 12 we can see the result for several different values for l and they show in general the properties which we have expected.

First of all the FWM peak basically around zero for odd l and around one for even l which could be explained by the limit of the Legendre polynomials for an angle of 180° between the two tagged jets in the previously defined region 1. This property gets nearly lost for higher l because region 1 shrinks and the events are more and more pushed into region 2.

Due to growth of region 2 with higher l, the peaks and cuts by which the borders between the regions were defined are more visible than before. Remarkable is that for odd values of l the peak is more dominant than it is for the sharp cut characteristic of even l. The reason is that the FWM in the 2-jet case for an angle of 180° for odd l start at zero followed by a maxima while for even l they start at one followed by a minima. So, with growing l the events will first see a maxima thus a peak for even l and a minima thus a sharp cut for odd l.

We also can observe that there are events in region 1 for even l and we can state that these events must be three or more jet events because in the 2-jet case this region was not accessible.

A very important observation is that we can still see some differences between WBF and background. Especially the $t\bar{t}$ production process is much broader than the WBF even if this process shows in general nearly the same behaviour after the kinematic cuts than WBF.

For small values of l the differences between the processes are small and they are getting bigger for growing values of l. However for even higher values of l the processes are again more and more matching each other up to a point where they are no longer distinguishable. For high l region 1 and 3 are small so that nearly all events are in region 2. But this region is strongly oscillating due to the Legendre polynomials and so the exact value of an event can't give any information about the jet correlations or about the process itself.

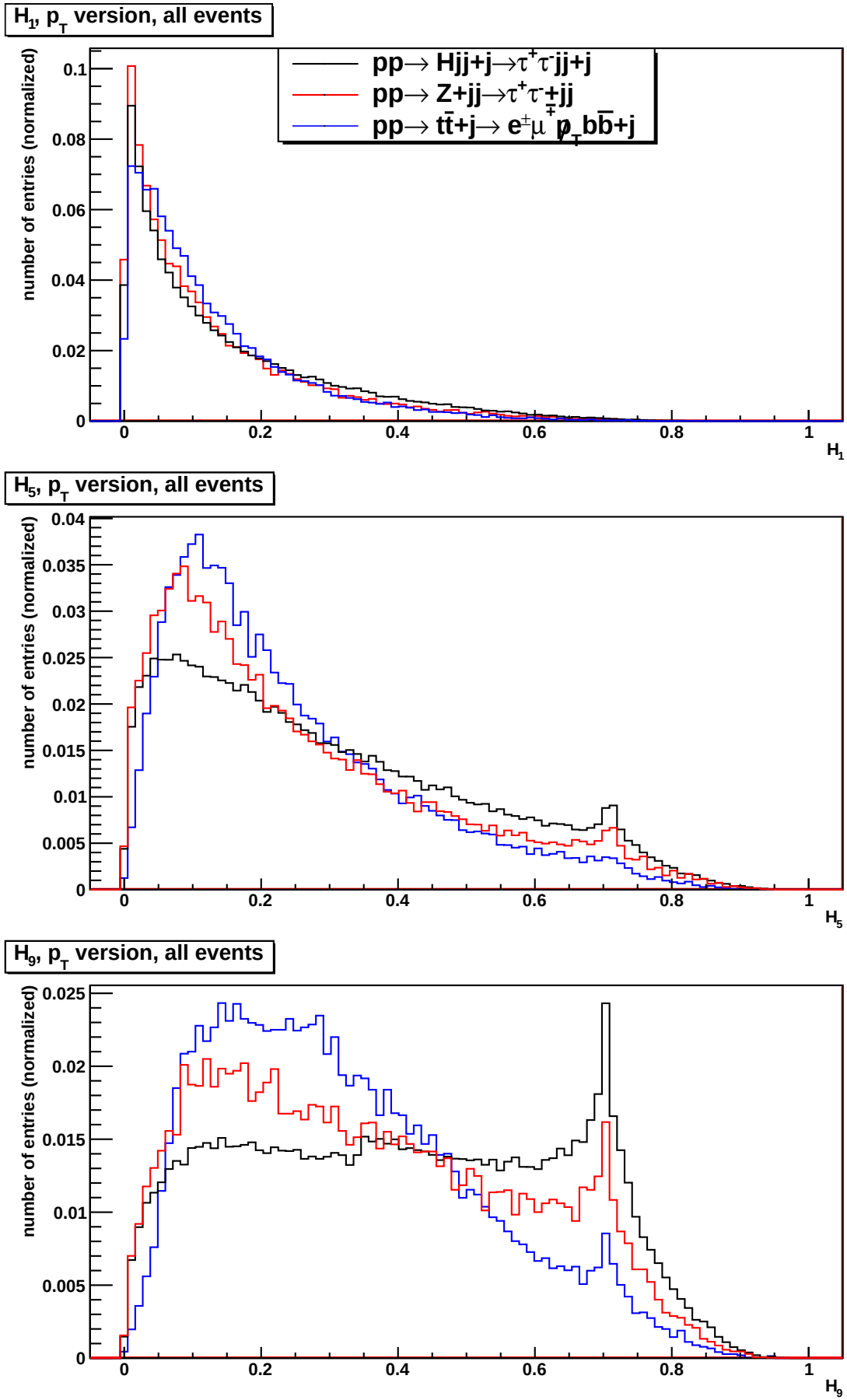

Figure 11: Applied FWM after all kinematic cuts for several odd values of l and p_T as the weight factor for WBF (black), Z+jets (red) and $t\bar{t}$ production (blue)

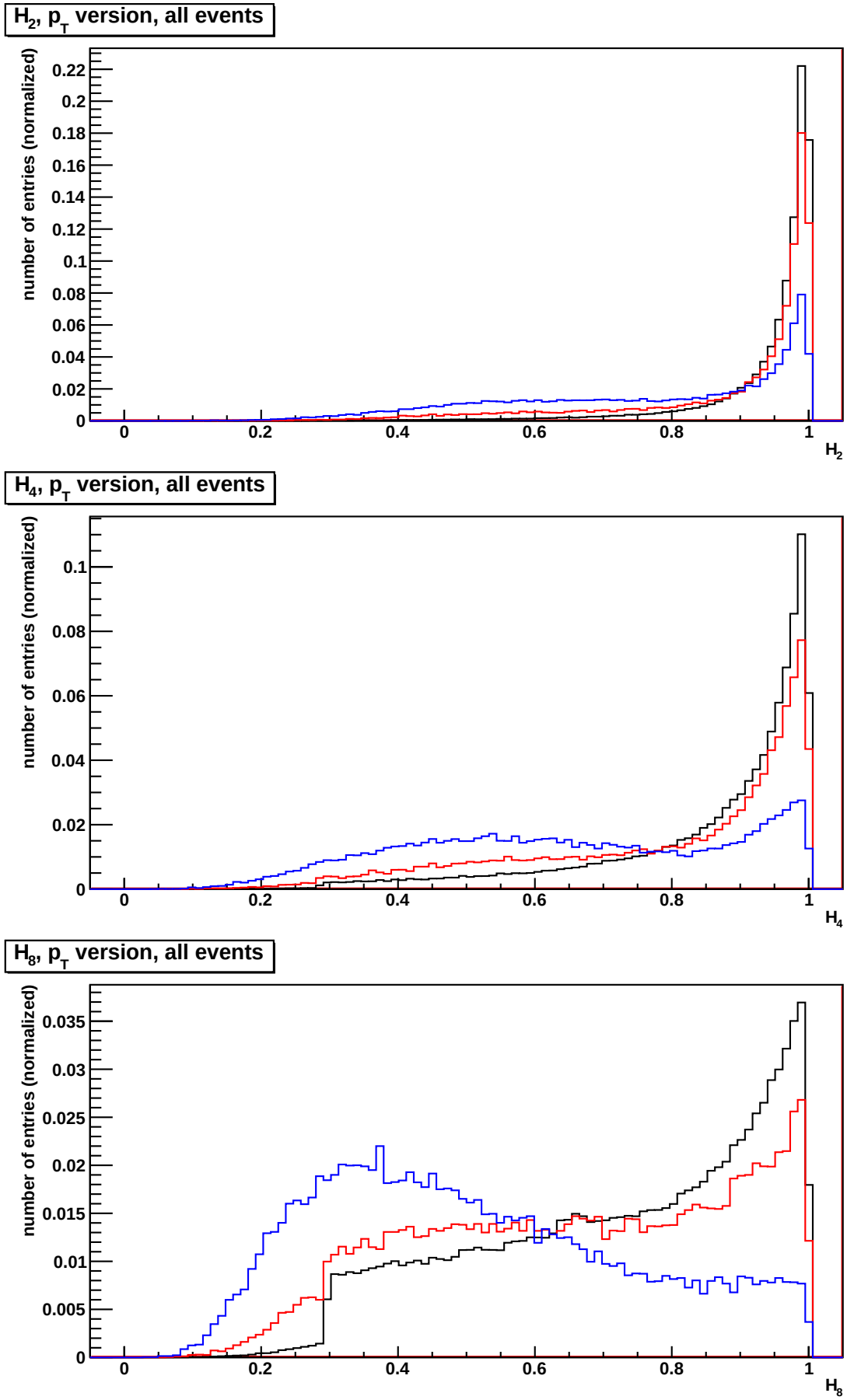

Figure 12: Applied FWM after all kinematic cuts for several even values of l and p_T as the weight factor for WBF (black), Z+jets (red) and $t\bar{t}$ production (blue)

7.1.2 2-jet Versus 3-jet Events

Let us now focus on the differences between 2-jet and 3-jet events. In Figure 13 we can see in the 2-jet case the shape of the FWM of the background processes are essentially the same as the shape of the WBF process. It's no wonder that there is no difference visible because the kinematic cuts are always applied to the tagging jets thus the properties of the leading jets should be approximately the same.

This leads to the conclusion that the above mentioned differences in the FWM for the different processes are mainly just due to the 3-jet events as we can see again in Figure 13. Here the same distinction like in Figure 12 and Figure 11 between the processes can be observed but are even stronger.

Notice that both backgrounds Z+jets and $t\bar{t}$ production have the same shape in 2-jet and 3-jet events but that the composition is different. This can be explained by the different amount of 2-jet and 3-jet events (see Table 3) and so they have different weights. For this reason the composed FWM shape of $t\bar{t}$ production shows mainly the 3-jet event shape while Z+jets is dominated from the peak in the 2-jet event shape.

7.2 QCD Jet Correlation

As we have seen the differences in FWM are mainly due to the 3rd jet which allows us to draw conclusions regarding the extra QCD jet. In Figure 13 we can see that the shift between a 3-jet and a 2-jet event is weak for odd l and much stronger in case of an even l. This is quite plausible by remembering that this shift is exactly the correction factor

$$\delta H_l^{(\text{3rd jet})} = \frac{2r_3}{(1+r_2)^2}\left(P_l^{13} + r_2 P_l^{23} - (1+r_2)H_l^{(\text{2-jets})}\right) + \mathcal{O}(r_3^2) \tag{7.1}$$

of eq.(6.45) and we have already mentioned this property. So let us focus on even l and discuss the formula for $\delta H_l^{(\text{3rd jet})}$.

On average the parameter r_2 should be the same for all processes because of the kinematic cuts and also the average value $H_l^{(\text{2-jets})}$ is the same, as we have seen previously in Figure 13. So we have to explain the differences between the processes with the angle of the QCD jet relative to the tagging jets which goes into the calculation of P_l^{13} and P_l^{23}. We can state that like in the 2-jet case the influence of the Legendre polynomials is stronger than the ratio r_3.

The 3-jet Fox-Wolfram distribution of WBF has a peak not far away from the maximum in the 2-jet event case. This lead to the conclusion that

$$\delta H_l^{(\text{3rd jet})} \propto P_l^{13} + r_2 P_l^{23} - (1+r_2)H_l^{(\text{2-jets})} \tag{7.2}$$

has to be more likely small thus the Legendre polynomials P_l^{13} and P_l^{23} have to be high enough to cancel the $H_l^{(\text{2-jets})}$ factor which is mainly around one.

Both leading jets are nearly back to back and forward-backward so $\cos\Omega_{13} \approx -\cos\Omega_{23}$ thus $P_l^{13} \approx (-1)^l P_l^{23}$. This lead to the appoximation:

$$\delta H_l^{(\text{3rd jet})} \propto P_l^{i3} - H_l^{(\text{2-jets})} \tag{7.3}$$

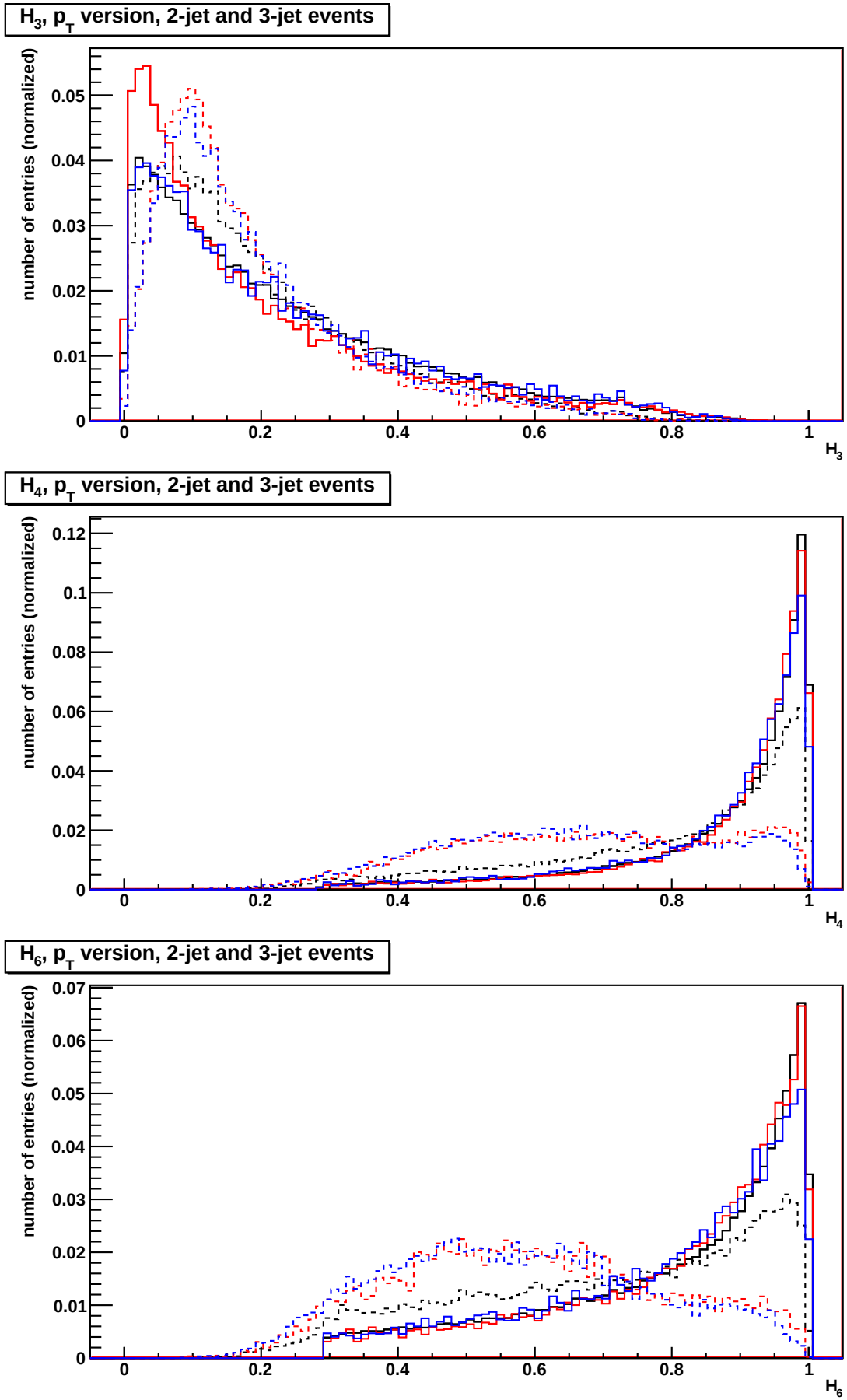

Figure 13: Comparision between 2-jet (solid line) and 3-jet (dotted line) events for WBF (black), Z+jets (red) and $t\bar{t}$ production (blue).

for even l and i either 1 or 2.

From $\delta H_l^{(\text{3rd jet})} \approx 0$ and $H_l^{(\text{2-jets})} \approx 1$ follows $P_l^{i3} \approx 1$ and so

$$\cos \Omega_{i3} \approx \pm 1. \tag{7.4}$$

We can deduce from eq.(7.4) that the 3rd jet must be close to one of the tagging jets which means that the extra parton is radiated under small angle. Remembering the topological structure of the WBF process this behaviour makes sense.

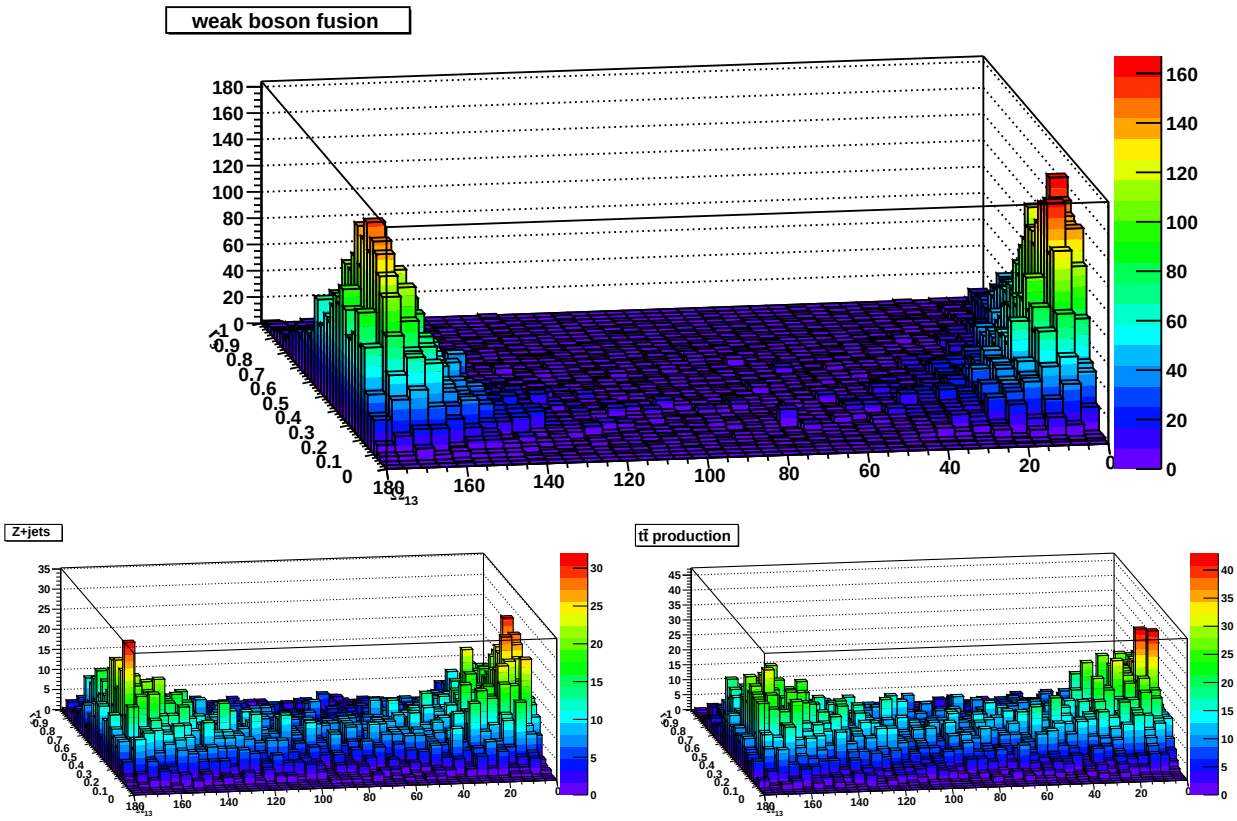

Figure 14: r_3-Ω_{13} plot for the different processes where the number of events is quantified by color. We can see the small angle radiation in case of WBF and the much more randomly distributed jet in case of the backgrounds

From the relatively broad distributions of the background processes in the 3-jet distributions we can surmise that there is no clear pattern underlying the distribution of the relative angle of the QCD jet. Thus the extra jets are more randomly distributed in space. Looking a bit closer, we can see a small bump at the same positions as in WBF. This leads to the conclusion that the 3rd jet is mainly distributed randomly but the probability for a small angle radiation is a bit higher.

This information is gathered only from the FWM but we can perform a cross check by plotting the real r_3-Ω_{13} dependency of the extra QCD jet for the different processes and compare it with our assumptions.

In Figure 14 we recieve confirmation of the information gathered from the FWM. Indeed the QCD jet is as expected radiated only under a small angle while the

background processes are more randomly distributed. But we can also see a small enhancement for radiation under small angles in case of the background processes which is possible to observe in the FWM.

7.3 Choice of Weight Factor

Now that we have finally analysed the FWM and explained the main origins of their shape, let us now answer the question why transverse momentum p_T was used as the weight factor instead of the total momentum $|\vec{p}|$ of the original definition.

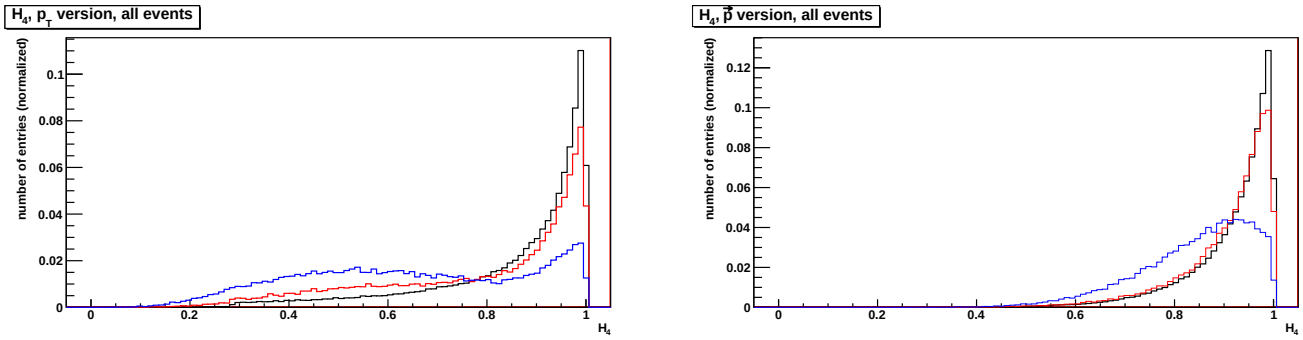

Figure 15: Comparision between the two different weight factors p_T (left) and $|\vec{p}|$ (right) with $l = 4$

In Figure 15 a comparison between the different weight factors p_T and $|\vec{p}|$ can be found. The general shape stays the same but the distinction between the processes are smaller and in this application the reason is quite simple.

As we have seen before the major difference between the processes, which leads to different shapes in FWM, is the 3rd jet. This 3rd jet can be in case of the background processes central while this is suppressed in WBF and due to the higher p_T of the central jets they are weighted more in the calculation of the FWM than forward or backward jets. So using p_T is a possible way to carve out the differences in the 3rd jet between the processes which is not as easy if using $|\vec{p}|$ as a weight factor.

Notice that in case of p_T as a weight factor we are losing the spherical symmetry of the FWM which was given in case of $|\vec{p}|$.

8 Conclusion

In the former sections we have seen the most important properties of the FWM. We've found out that the they are bounded ($0 \leq H_l \leq 1$) and that in case of two jets we can rewrite the FWM such they are depending only on two parameters, r and Ω. By defining three different regions and taking a closer look to the maxima and minima of the analytical expression it was possible to explain the dominant shape of the FWM and their characteristic traits. Already at this stage it is possible to make statements about the correlation between the two leading jets. In this way we could predict the shape in the case of the two forward-backward jets of WBF. Any additional jet can be regarded as a shift to this 2-jet FWM.

Applying the FWM to WBF events and backgrounds generated by SHERPA we were able to observe this shift between 2-jet and 3-jet events directly. To some approximation it was possible to deduce that the 3rd jet must be close to the leading jets in WBF while they are more randomly distributed in space in case of the backgrounds. Due to the fact that the 3rd jet refers mainly to an extra QCD jet added to the process this behaviour is quite reasonable because it is in conformation with theory. By using p_T instead of $|\vec{p}|$ it is possible modify the FWM such that they no longer as spherically symmetric. Hence the FWM become more sensitive to the central QCD jets of the background and so to enhance the differences between the processes.

We can state that the FWM are quite sensitive to the correlations between the leading jets - specifically to their relative spacial angle. Because the FWM are a set of event shape observables the choice of the parameter l allows it to make sophisticated qualitative statements. A quantitative analysis is limited by the amount of parameters inasmuch n new parameters for the n-th additional jet are going into the calculations.

The fact that the FWM depend on the behaviour of the extra QCD parton can be used to make some further distinction between the processes by cutting on the FWM. However achieving a good enhancement is constricted by the overlay of the distributions of the different processes.

In future projects one can take a closer look to FWM because even though it was possible to explain the general shape many dependencies can be elaborated more carefully. Some of these dependencies might offer some different applications than gathering information about the 3rd jet, e.g. the $\Delta\varphi$ dependency is a interesting candidate because of its importance for actual physical questions [17].

References

[1] Wikimedia Commons, `http://commons.wikimedia.org/wiki/File:Standard_Model_of_Elementary_Particles.svg` (August, 30 2012).

[2] bwGRiD (http://www.bw-grid.de), member of the German D-Grid initiative, funded by the Ministry for Education and Research (Bundesministerium für Bildung und Forschung) and the Ministry for Science, Research and Arts Baden-Wuerttemberg (Ministerium für Wissenschaft, Forschung und Kunst Baden-Württemberg).

[3] Wikimedia Commons, `http://commons.wikimedia.org/wiki/File:Legendrepolynomials6.svg` (August, 30 2012).

[4] *"OpenMP Application Program Interface, Version 3.1"*. OpenMP Architecture Review Board, July 2011.

[5] Rene Brun and Fons Rademakers. ROOT - An Object Oriented Data Analysis Framework. *Nucl. Inst. & Meth. in Phys. Res.* **A 389 (1997) 81-86.**, Proceedings AIHENP'96 Workshop, Lausanne, Sept. 1996, See also http://root.cern.ch/, 1997.

[6] M. Cacciari, G.P. Salam, and G. Soyez. "The anti-k_T jet clustering algorithm". *JHEP* **04** *(2008) 063*, 2008.

[7] M. Cacciari, G.P. Salam, and G. Soyez. "FastJet User Manual". *EPJC* **72** *(2012) 1896.* **arXiv:1111.6097**, Nov. 2011.

[8] F. Gianotti (ATLAS Collaboration). "Expected Performance of the ATLAS Experiment". *arXiv:hep-ex/0901.0512v4*, 2008.

[9] F. Gianotti (ATLAS Collaboration). "Update on the Standard Model Higgs search in ATLAS". *ATLAS-CONF-2012-093*, July, 4 2012.

[10] J. Incandela (CMS Collaboration). "Update on the Standard Model Higgs search in CMS". *CMS-PAS-HIG-12-020*, July, 4 2012.

[11] M. Dobbs and J.B. Hansen. "The HepMC C++ Monte Carlo Event Record for High Energy Physics". *Comput. Phys. Commun.* **134** *(2001) 41*, 2001.

[12] J. Beringer et al. (Particle Data Group). *Phys. Rev.* **D86***, 010001 (2012)*, 2012.

[13] R.D. Field, Y. Kanev, and Tayebnejad. Topological analysis of the top quark signal and background at hadron colliders. *Phys. Rev* **D55**, pages 5685–5697.

[14] G.C. Fox and S. Wolfram. "Event Shapes in e^+e^- Annihilation". *Nucl. Phys.* **B149**, pages 413–496, 1979.

[15] L. Garren, I.G. Knowles, T. Sjöstrand, and T. Trippe. "Monte Carlo Particle Numbering Scheme". April 2002.

[16] T. Gleisberg, S. Höche, F. Krauss, M. Schönherr, S. Schumann, F. Siegert, and J. Winter. "Event generation with SHERPA 1.1". *JHEP* **02** *(2009) 007*, 2009.

[17] K. Odagiri. "On azimuthal spin correlations in Higgs plus jet events at LHC". *arXiv:***hep-ph***/0212215v2*, 2003.

[18] T. Ohl and T. Darmstadt. "feynMF: Drawing Feynman Diagrams with LATEX and METAFONT". 1995.

[19] T. Plehn, D. Rainwater, and D. Zeppenfeld. "Method for identifying $H \to \tau\tau \to e^{\pm}\mu^{\mp}\not{p}_T$ at the CERN LHC". *Phys. Rev.* **D61***, 093005*, 2000.

Acknowledgments

First and foremost I would like to give special thanks to Catherine Bernaciak who always takes time for us and answered our questions with patience whenever we had one. Furthermore I want to thank my supervisor Tilman Plehn who came up with the idea working on the FWM and thus giving me the great opportunity to get an insight into actual research. Of course I also want to thank Anja Butter for working together on this project and for the many hours of inspiring discussions. Last but not least I want to give my thanks to the whole research group for interesting conversations during lunch and tasteful cakes.